

EMPIRICAL AND NUMERICAL MODELING OF T-PHASE PROPAGATION FROM OCEAN TO LAND

Jeffry L. Stevens, G. Eli Baker, and Ron W. Cook
Maxwell Technologies, Systems Division
Gerald D'Spain and Lewis P. Berger
Marine Physical Laboratory, Scripps Institution of Oceanography
Steven M. Day
San Diego State University

Sponsored by the Defense Threat Reduction Agency

ABSTRACT

T-phase propagation from ocean onto land is investigated by comparing data from hydrophones in the water column with data from the same events recorded on island and coastal seismometers. The threshold level for hydroacoustic signals measured in the SOFAR channel is much lower than the threshold for T-phases observed on island and coastal seismic stations. Because nearly half of the future hydroacoustic network of the International Monitoring System is made up of T-phase stations on land, it is important to understand T-phase propagation onto land in order to evaluate the capability of the hydroacoustic network to monitor the oceans. To estimate the transfer function, it is necessary to find events with large enough T-phases to be measurable over an acceptable frequency band at land-based stations near a hydroacoustic station.

A particularly good data set has been obtained for the series of events from the emerging seamount Loihi, located southeast of Hawaii. These events generated very large amplitude T-phases that were recorded at both the IMS hydrophone stations and land based stations near the northern California coast and over 100 km inland from the coast. We have obtained data from the preliminary IMS hydrophone station at Point Sur, from land based stations operated by U. C. Berkeley along the coast of California, and from the PG&E coastal California seismic network, and used this data set to estimate the T-phase transfer functions for all of these paths.

The transfer function and predicted signal from the Loihi events are modeled with a composite technique using normal mode based numerical propagation codes to calculate the hydroacoustic pressure field and an elastic finite difference code to calculate the seismic propagation to land-based stations. The modal code is used to calculate the pressure field in the ocean off of the California coast, which is used as input to the finite difference code TRES to model propagation onto land. Animations were created from the finite difference calculations to help visualize the complex conversion process.

We also look at the nature of T-phases after conversion from ocean to land by examining far inland T-phases. We find that T-phases propagate primarily as P-waves once they are well inland from the coast, and can be observed in some cases hundreds of kilometers inland from the coast.

Key Words: Hydroacoustic, T-phase, Finite Difference, IMS, Loihi

OBJECTIVE

The objective of this project is to better understand the propagation of T-phases from ocean to land, and the performance of T-phase International Monitoring System (IMS) stations, through empirical and numerical methods. The empirical study uses data from pressure sensors in the ocean and coastal and island seismometers to examine the T-phase transfer function. The numerical study uses finite difference calculations to model propagation of T-phases from ocean to land.

RESEARCH ACCOMPLISHED

The International Monitoring System (IMS) hydroacoustic network is a relatively sparse network consisting of 6 underwater hydroacoustic stations and 5 land-based seismic T-phase stations. The hydroacoustic stations are much more sensitive to underwater signals than the T-phase stations and have a higher sampling rate and broader frequency range. The broader frequency range is important for identifying explosions, which are characterized by higher frequency content than other sources. Because of these limitations, it is important to understand the efficiency of T-phase conversion in order to assess the capabilities of the IMS network for detection and identification of underwater sources. Currently, only part of the hydroacoustic network is in place, and an additional hydroacoustic station at Point Sur is acting as part of the IMS network. Figure 1 shows the location of the two hydroacoustic and one T-phase stations which are currently operating in and adjacent to the Pacific Ocean, and the location of the emerging seamount Loihi, which has been the source of strong T-phases.

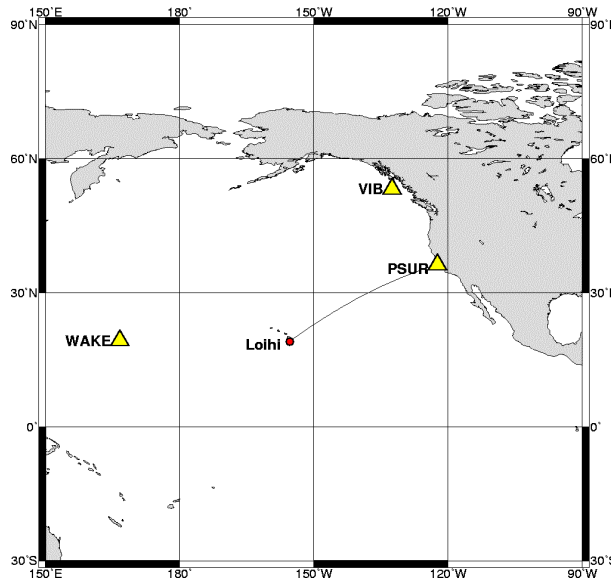


Figure 1. Hydroacoustic network stations in the current International Monitoring System in the Pacific Ocean. VIB is a T-phase station. Point Sur and Wake are underwater hydroacoustic stations. “Loihi” marks the location of strong T-phase sources south of Hawaii used in this study. The great circle path from Loihi to Point Sur is also shown.

Transmission of T-phase Energy from the Ocean onto Land

We have gathered data sets from events that were recorded on both underwater and coastal seismic stations for the purpose of directly measuring T-phase conversion. Several earthquakes from the emerging seamount Loihi and on the island of Hawaii generated very strong T-phases that impacted the California coast. We have collected recordings of these events from the Point Sur (PSUR) hydroacoustic station, the Pacific Gas and Electric Central Coast seismic network (PG&E), and the Berkeley broadband digital seismic network (BDSN). The location of these stations and the bathymetry of the California continental shelf are shown in Figure 2. This is a nearly optimal situation for study of T-phase conversion because the hydroacoustic waves impact the coastline almost perpendicular to the coast as shown by the ray path on Figure 2.

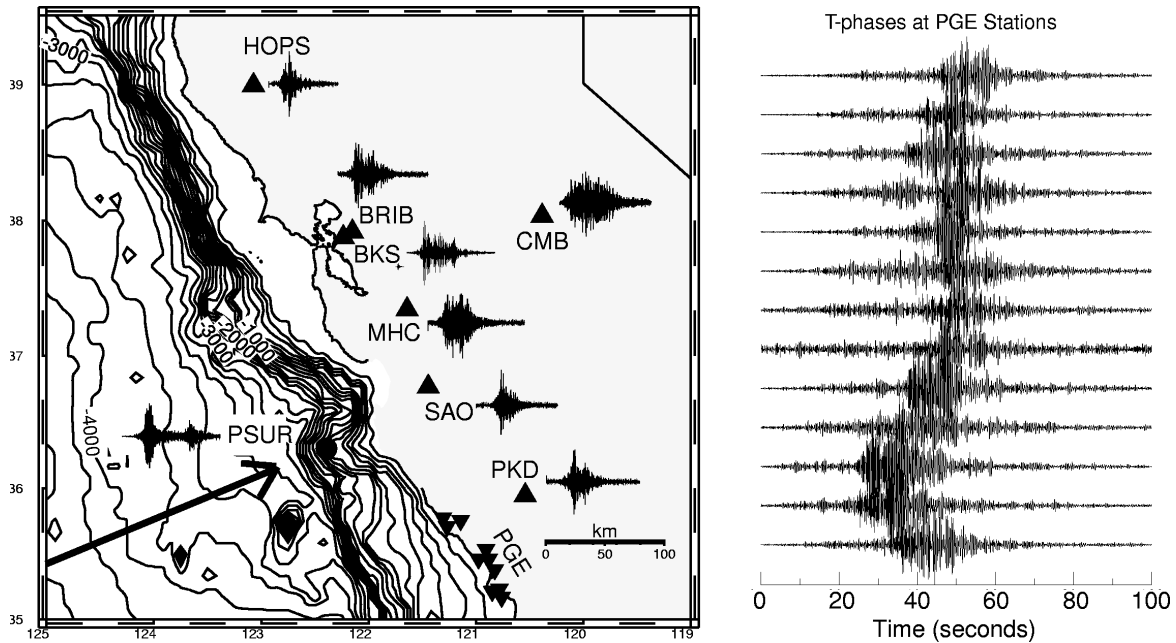


Figure 2. Records from the 1997 June 30 Loihi event and station locations. The propagation direction is indicated by the arrow, which points to the hydroacoustic station PSUR (indicated by the circle). 150 seconds of the T-phase record is shown to the station's left. The BDSN stations (large triangles) and corresponding records are included on the map on the same scale. The PG&E station locations are indicated by inverted triangles and their waveforms are shown to the right, in order of increasing distance from bottom to top. The arrival times do not correspond well to total distance because the distance from the conversion point varies. The bathymetry is contoured in 200 m intervals.

The sampling rate and instrumentation are different for each of the three networks. Point Sur is sampled at 200 samples per second and the instrument response is approximately proportional to frequency at frequencies less than 25 Hz. Data in the BDSN network is sampled at 20 samples per second. BDSN instrument responses are approximately flat to velocity in the 1-10 Hz frequency band. The PG&E network consists of S-13 seismometers with a sampling rate of 100 samples per second, and is flat to velocity from 2-25 Hz. We have relative gain corrections for each of the instruments, however the absolute gain for the PG&E stations is uncertain. Because of the differences in instrumentation, the usable frequency band for obtaining T-phase transfer functions from this complete data set is about 2 to 9 Hz.

We have calculated T-phase transfer functions for this data set by taking the ratio of the instrument corrected vertical component velocity spectral amplitudes of the seismic stations to the instrument corrected Point Sur pressure spectra for all good quality data at the PG&E stations and the 6 coastal BDSN stations (CMB was excluded because it is much farther inland). The spectral ratios were averaged for all events for each station. The resulting spectral ratios are shown in Figure 3. There is a clear decline in amplitude with frequency for both networks, but it is particularly pronounced for the BDSN network. This is likely due to greater attenuation of the higher frequencies because of the longer paths to the BDSN stations. Simulations discussed later in this paper indicate that much of the energy in the hydroacoustic wave is transmitted to land at approximately 200 m bathymetry, which corresponds to the contour line (Figure 2) nearest the coast. The crustal paths from the conversion point to the PG&E stations are only 5 to 20 km long, while paths to the BDSN stations are 40-75 km.

Although the transfer function can only be calculated by numerical methods, we can estimate an approximate upper bound on the transfer function by considering the simple case of a plane acoustic wave travelling in the ocean and propagating into a solid at normal incidence. This is an approximate upper bound in the sense that any scattering or other boundary effects will reduce the amplitude below this level, although conversion to shear waves or focusing could conceivably cause amplitudes to exceed this value. For propagation of a plane wave at normal incidence from a fluid into a solid, the transmission coefficients for velocity and pressure are given by:

$$T_{v_f v_s} = \frac{2\rho_f \alpha_f}{\rho_s \alpha_s + \rho_f \alpha_f} \quad T_{p_f v_s} = \frac{2}{\rho_s \alpha_s + \rho_f \alpha_f}$$

where ρ and α are the density and compressional velocity and the subscript s indicates solid and f indicates fluid.

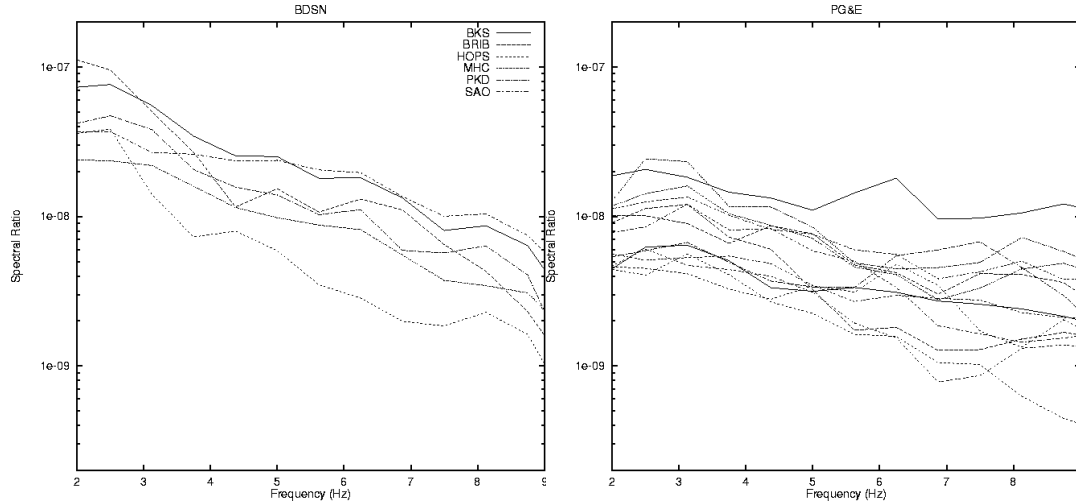


Figure 3. Ratios of seismic spectra at stations in California that recorded the Loihi events, divided by the Point Sur spectra. These are T-phase transfer functions converting pressure to vertical velocity. The frequency band shown here is from 2-9 Hz. the left figure shows BDSN stations and the right figure shows PG&E stations. There is some uncertainty about the absolute amplitude of the PG&E records, however the amplitude of the BDSN records, and the spectral shape of both sets of curves, are accurate. Spectral ratios are in MKS units (meters/second/Pascal).

Depth (m)	P velocity (m/s)	S velocity (m/s)	Density (kg/m ³)
500	3400	1500	2200
1500	5000	2900	2500
11000	6100	3484	2750
21000	6300	3503	2800
31000	6600	3464	2900
×	8000	4260	3300

Table 1. Velocity model for the California coast.

Table 1 lists a velocity model for the California coast near Point Sur from Mooney et al (1998) with the shear velocity as modified by Stevens and McLaughlin (1997). Using a typical water velocity and density of 1480 m/s and 1000 kg/m³, respectively, we can estimate upper bounds on the velocity transfer function of 0.21 and 0.36 for the top two layers of the coastal California earth model. The pressure to velocity transfer function for each layer has an upper bound of 1.4x10⁻⁷ and 2.4x10⁻⁷ meters/second/Pascal. At 2 Hz, the average of the BDSN spectral ratios is 0.6x10⁻⁷, about a factor of 3 less than the estimate given above, which gives a numerical estimate of the efficiency of T-phase transmission into the coast. That is, the BDSN records show that at low frequencies the transfer function is reduced by complex coastal interactions by a maximum of about a factor of 3. The spectra of the BDSN records fall off by an order of magnitude over the 2-9 Hz frequency band. The PG&E records show that for stations close to the coast, the maximum attenuation with frequency is a factor of 3-4 over the 2-9 Hz frequency band.

Far Inland T-phases

The ocean hydroacoustic phase may convert to a variety of complex phases due to the interaction with the coast. We can get some insight into the type of conversion that occurs by looking at far inland T-phases, and examining the propagation speeds of these waves. The T-phase from the 1997/06/30 event was large enough to be observed as much as 200 km inland from the coast. Figure 4 shows two sets of seismograms recorded along two (approximate)

great circle paths. The paths are from SAO to KCC and from JRSC to MHC to CMB. Since the waveform is dispersed, there is some uncertainty about when to pick the arrival, however if we use the peaks of each wave train, then we get a velocity between SAO and KCC of 6.8 km/sec, and a velocity along the path of the other three stations of 5.6 km/sec. These velocities correspond to P-wave speeds, so the T-phases must be travelling as P-waves over this range.

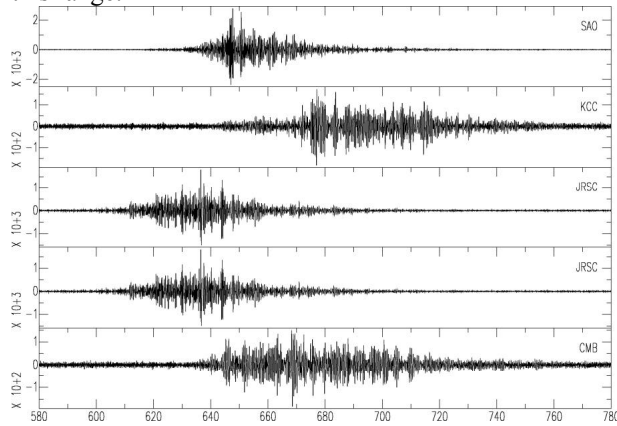


Figure 4. T-phases recorded near the coast and far inland from the 1997 June 30 Loihi event. The top two seismograms are from stations located along one great circle path and the bottom three seismograms lie along a second great circle path. The horizontal axis is time in seconds. The data has been high pass filtered at 2 Hz.

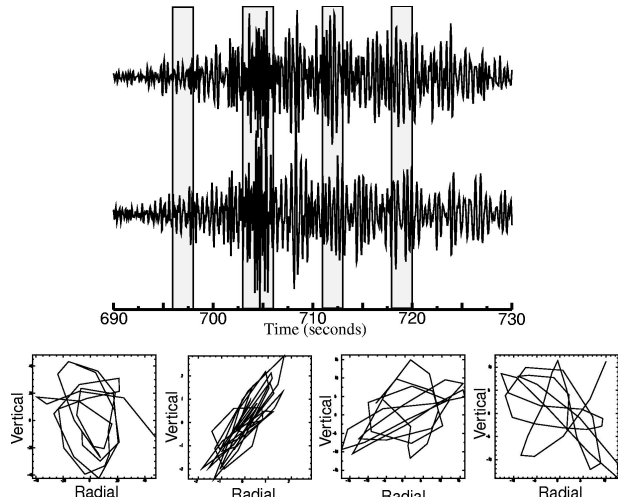
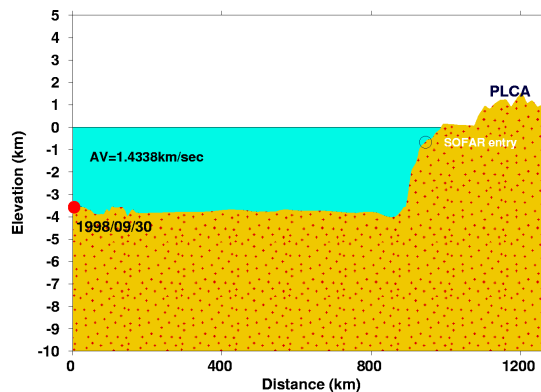
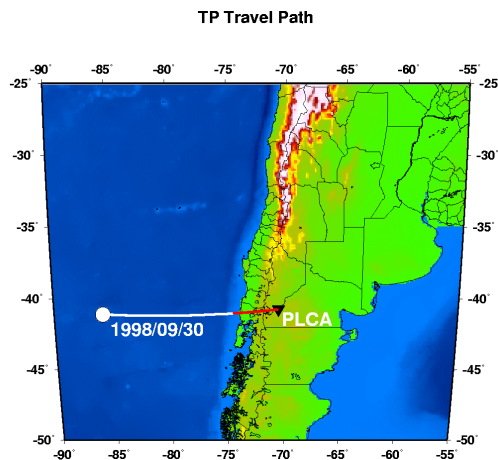


Figure 5. Vertical (top trace) and radial (lower trace) component seismograms from SAO for the 1997 June 30 event. Particle motions for four time windows outlined by shading are shown below the seismograms. The linear motion of the second time window indicates dominance by body waves, and the elliptical motion of the first time window suggests that the early part of the wave train is composed of surface waves.

Particle motion provides an independent means of assessing wave type. Figure 5 shows that the particle motion for the largest part of the record, near the front of the T-phase, is strongly linear. This part of the record is clearly dominated by body waves, most likely P-waves, in agreement with the conclusion from travel times. Linearity decreases later in the record, although it's not clear whether that is due to the arrival of later scattered P-wave energy, surface wave arrivals, or a mixture of phases. The particle motion of the earliest part of the T-phase is elliptical and retrograde, suggesting that this part of the wave train is composed of Rayleigh waves. This is consistent with the simulations shown later in this paper, which indicate that surface waves can precede the P-wave near the coast, due to earlier conversion of the T-phase in water to surface waves.



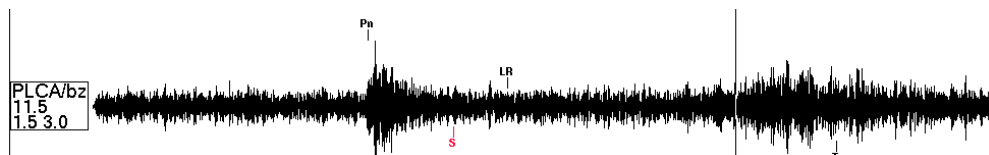


Figure 6. Map (left) and bathymetry/topography (right) for the path of T-phases from the 1998/09/30 earthquake recorded at PLCA. At the bottom is the seismogram recorded at PLCA with the phases marked.

Cook and Stevens (1998) collected a number of examples of T-phases recorded far inland from the coast. We show one example of these here. Figure 6 shows a T-phase from an earthquake in the eastern South Pacific ocean recorded in Argentina, on a path that traveled through the Andes and over a distance of approximately 300 km on land. The velocity labeled “AV” on the plot is the apparent velocity in the water after subtracting the travel time for propagation on land. This apparent velocity acts as a consistency check and should be close to the velocity of water if the T-phase is traveling on land at Pn speeds. This is additional evidence that T-phase propagation on land, at least once the wave has propagated well inland from the coast, consists of P-waves. Far inland T-phases have very peculiar travel times because they travel very slowly (~ 1.4 km/s) in the ocean, and very fast (up to 8 km/sec) as P-waves on land. Consequently, the T-phase starts out far behind the other seismic phases, but will eventually catch up to the Rayleigh wave if it travels far enough. Because of this, there is some danger in a semi-automated processing system like the IDC that T-phases could be misidentified as other phases.

Numerical simulations of T-phase Transfer functions

In order to better understand the T-phase transfer functions, and the nature of the seismic T-phase as compared the direct hydroacoustic signal, we have performed numerical simulations of the waveforms and the transition process. A more detailed description of this work is given by Stevens et al. (1999). Because of the excellent data set for the Loihi events, we are modeling waveforms that travel from Loihi to the California coast traveling through the location of the Point Sur hydroacoustic station. The map in Figure 1 shows the locations of the Loihi seamount southeast of the Hawaiian Island chain and the Pt. Sur station on the continental slope just to the southwest of Monterey Bay on the central California coast. The two locations are separated by a distance of 3745 km. Bottom bathymetry data along the path was obtained from the National Geophysical Data Center. The water depth is nominally 5000 m along the propagation path until the continental slope along the west coast of California is reached. In the region being modeled near Point Sur, a single typical profile having a sound speed of 1525 m/sec at the surface and 1482 m/sec at the sound channel axis at 700 m depth was used. 9 distinct temperature profiles were used to model the path between Loihi and Point Sur.

Kraken, a normal mode code written by M. Porter, was used to calculate the hydroacoustic wave field off the coast of California. Kraken can be obtained through the Ocean Acoustics Library web site at <http://oalib.njit.edu/>. To model the range dependence, the propagation path has been divided into 48 consecutive range-independent segments. The range intervals for the segments are determined by the places where the bottom bathymetry contours change by 100 m. 18 segments were used on the first 3710 km of the path, to the point where the solution was transferred to the finite difference calculation. The ocean bottom for the in-water propagation calculations is modeled as a lossy fluid layer of 1 km thickness with a compressional velocity of 2100 m/sec and density of 2100 kg/m³ overlying a lossy fluid halfspace with velocity 6000 m/sec and density 2700 kg/m³. The T phase source is modeled as a single omnidirectional point at a depth of 1 km, corresponding to the depth of the peak of the Loihi seamount.

The adiabatic approximation has been used in the normal mode numerical modeling to model propagation through the deep ocean. The problem is transferred to a finite difference code at the point where the ocean depth begins to decrease rapidly. The ocean water depth in this part of the calculation is shown in Figure 7, together with the number of modes that can exist at each integral frequency from 1 to 10 Hz over this range. As the ocean waveguide becomes progressively shallower, the water depth where a given mode at a given frequency reaches cutoff determines the location along the continental slope where that mode's energy couples into the land seismic field. Almost all of the modes couple into the bottom over the 80 km range from 3710 to 3790 km, with the majority of the higher order modes coupling in over the 35-km interval from 3715 to 3750 km, and the lower order modes in the 20-km interval from 3765 to 3785 km. It is over the corresponding depth interval for this latter range, i.e., depths shallower than 1000 m, that the elastic properties of the continental slope are most critical in modeling the ocean-

acoustic-to-land-seismic field coupling. A more detailed discussion of modal propagation in the ocean and modal coupling is given in D'Spain, et al (1999).

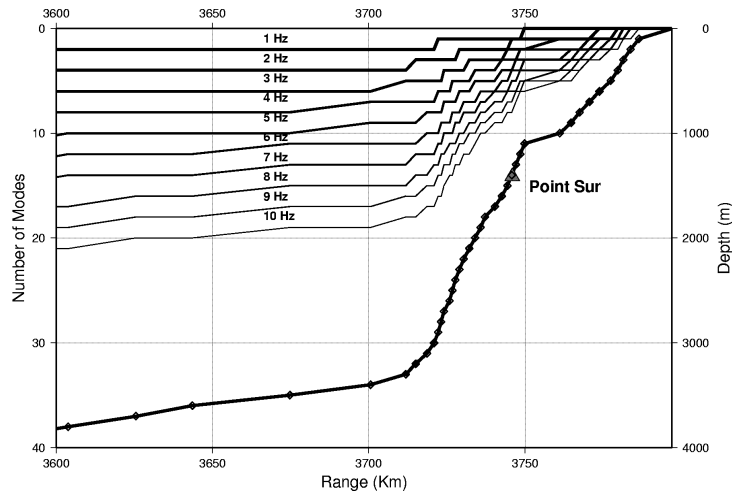


Figure 7. Number of in-water propagating modes at each frequency versus range. The bottom bathymetry also is shown as a set of connected diamonds. Each curve corresponds to a different frequency. The top curve corresponds to a frequency of one Hz, the second to two Hz, etc. At 10 Hz, 21 modes are supported at the deepest depth, while only two modes exist at 1 Hz.

Two-dimensional finite difference calculation of propagation onto land

We use the two-dimensional finite difference code TRES2D to model the propagation of hydroacoustic waves onto the coast. The Kraken normal mode solution in the ocean at a distance of 3710 km from Loihi was used as the source in the finite difference calculation. The first step in this process is to convert the modal spectra to time domain displacements and pressures at each node point. The first 20 seconds of the pressure waveforms at two depths are shown in Figure 8. At 1005 meters depth, the fundamental mode is much larger than the other modes, however at 2160 meters depth, the second mode is larger than the fundamental. The modes have been filtered in a band pass of 1.0 to 4.5 Hz, consistent with the spectral resolution of the finite difference calculation.

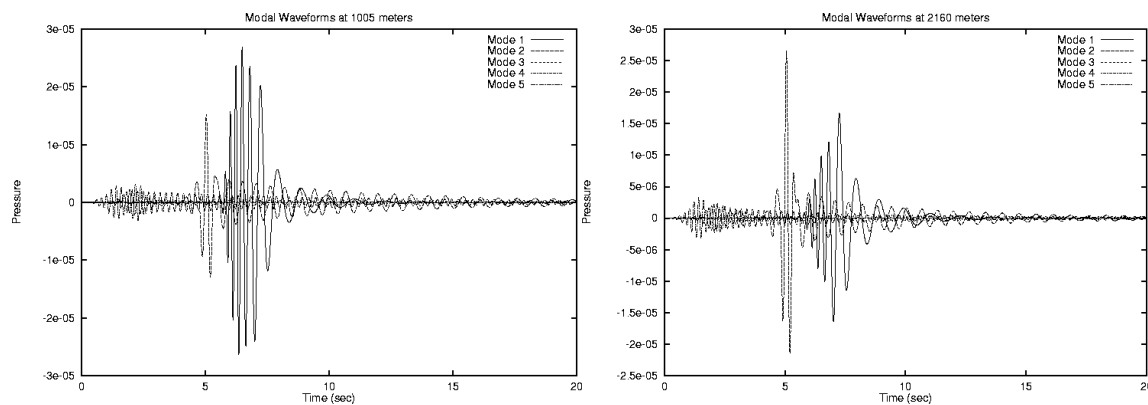


Figure 8. Input waveforms for first five modes at depths of 1005 (left) and 2160 (right) meters.

Even though this is a two-dimensional problem, it requires a very large calculation because the distances of interest are large, about 100 km, the wave speed in the water is slow, and we are interested in frequencies higher than 1 Hz. The velocity model is the California coastal model discussed earlier and listed in Table 1. The ocean model is based on the bathymetric profile along the path from Loihi through Point Sur and the water velocity profile in the ocean near Point Sur. We used a grid with a uniform spacing of 67 meters per grid cell, dimensions of 1500x500 grid blocks, and a time step of 0.005 seconds. The calculation was run for 20,000 cycles to obtain a duration of 100

seconds. The calculation should be accurate throughout the grid to at least 2.5 Hz. We expect to see some numerical dispersion in the 2.5-4.5 Hz frequency band in the lower velocity parts of the grid.

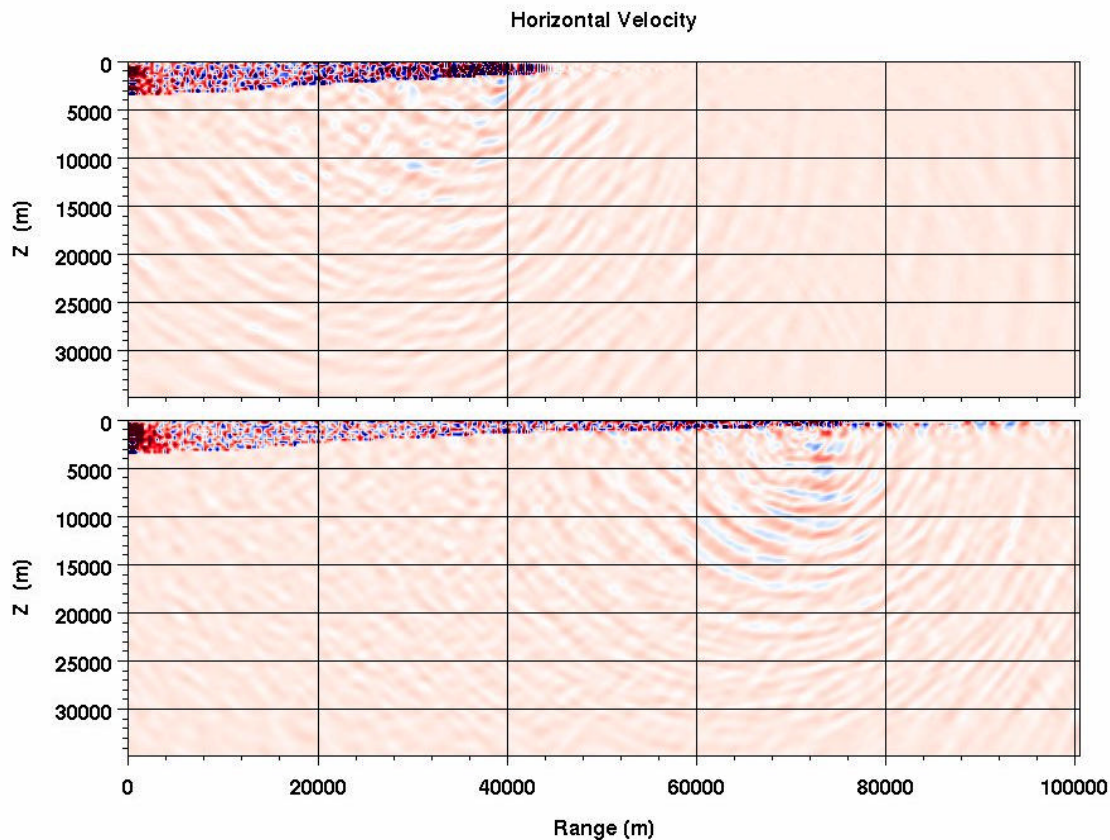


Figure 9. Snapshot of the calculation at 35 seconds (top) and 65 seconds (bottom). In the bottom figure, the dominant hydroacoustic arrival has reached a depth of 200 meters. At this point there is a burst of energy transferred as body waves from the ocean into land. Zero range corresponds to the point 3710 km from Loihi (see Fig. 18). The ocean/land interface at the surface is at location 87368.

Two calculations were performed, one with only the fundamental mode and one with the first 5 modes. Velocities for the full grid were saved for each second of time in the calculation, and these were used to create images and animations to help visualize the evolution of the velocity field. The results with a single mode and with five modes are very similar. There is a gradual decay of the hydroacoustic wave as it travels upslope, with body waves emitted continuously with varying amplitudes into the earth below, and a surface wave that gradually forms along the ocean bottom. At sharper bathymetric gradients the transmission is increased, and when the hydroacoustic wave reaches an ocean depth of 200 meters, there is a burst of energy much larger than anywhere else along the path. Strong surface waves are present on land from the edge of the ocean to the boundary of the calculation. Figure 9 shows snapshots of the fields at 35 seconds and 65 seconds. The second figure shows the burst of energy at 200 meter depth. Color animations of both calculations can be viewed online at <http://www.maxwell.com/products/geop/Movies/hydro.htm>. The calculated T-phases have some very odd properties. As can be seen in Figures 9 and 10, a strong surface wave develops quite early and can be seen on land at 65 seconds, which is the same time that the burst of body waves occurs. Consequently the surface wave appears in the wave train before, and simultaneous with, the body waves generated by the final decay of the hydroacoustic wave. The T-phase near the coast is therefore a mixture of seismic phases, similar to what was observed in Figure 5.

The results of the calculation were saved with a much finer time resolution at selected locations along the surface, and at a depth of 740 meters in the center of the sound channel. Figure 10 shows the calculated horizontal velocity in the water at 47235 m, which corresponds approximately to a location above the Point Sur hydroacoustic station. Also shown are the horizontal and vertical components of the waveform on the surface at location 87904 m, which is on land close to the coast. The amplitude ratios between the velocity on land and in the water are about 0.2, which

is consistent with our earlier estimates of the upper bound of the transfer function. The waveforms on land are complex and longer in duration than the underwater waveform, and are dominated by surface waves.

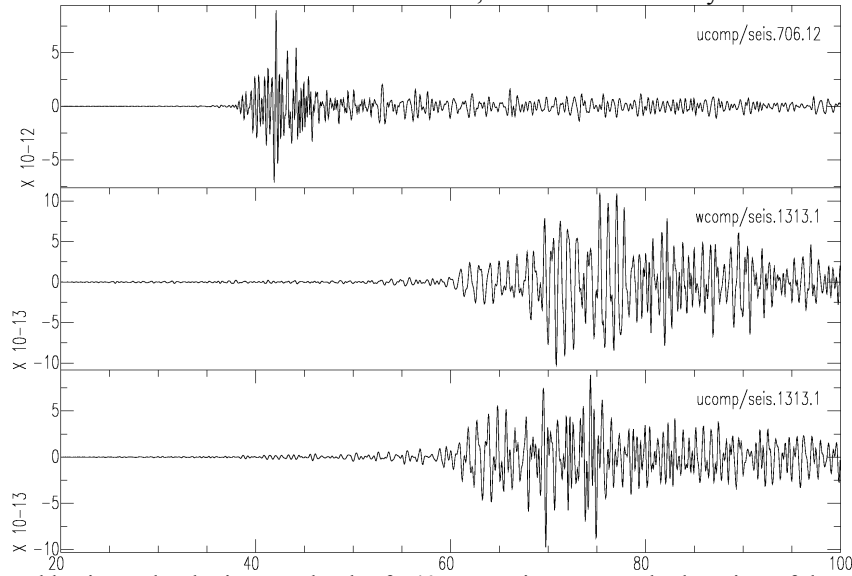


Figure 10. Calculated horizontal velocity at a depth of 740 meters in water at the location of the Point Sur station (top) and vertical (mid) and horizontal (bottom) components of the velocity on land close to the coast. Horizontal axis is time in seconds since the start of the calculation.

Figure 11 shows the spectral amplitude of the horizontal velocity in the 1-4 Hz frequency band underwater at the Point Sur location and the vertical velocity at a station on land close to the coast. The underwater spectrum is nearly flat across this frequency band. The spectra on land, however, exhibit a significant decline in amplitude with frequency, similar to the spectral decline observed for the coastal California stations. This suggests that during transmission from water to land, the higher frequencies are scattered more strongly than the lower frequencies, leading to a decline in high frequency content in the coastal waveforms.

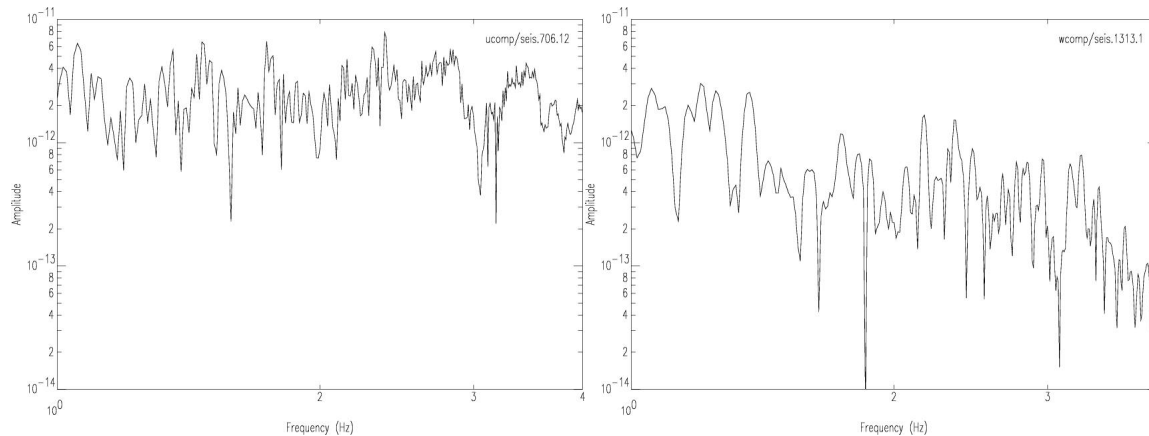


Figure 11. Calculated spectral amplitudes of the horizontal velocity at a depth of 740 meters underwater (top) and the vertical velocity at the surface on land near the coast (bottom).

Discussion

We have used T-phase observations in water and on land together with numerical calculations of T-phase propagation from water to land in order to understand the nature of T-phase conversion. The results are complex and at first glance contradictory. Whereas T-phases are observed to travel at P-wave speeds on land, the calculations show strong surface waves near the coast. However, the calculations also show lower amplitude body wave arrivals even very close to the coast, and strong body waves propagated away from conversion points along the ocean

bottom. Some of this body wave energy will return farther inland as Pg and Pn phases. The high frequency surface waves, on the other hand, can be expected to attenuate away very quickly and will not propagate to large distances. We therefore expect to see strong surface waves and smaller P-wave arrivals near the coast, with the surface waves dying out and the P-waves becoming dominant as the wave travels inland. The strong surface waves seen in this case may be somewhat anomalous, since they are formed in the ocean and propagate up the ocean bottom onto land. In a real earth with bottom sediments, these would be more strongly attenuated.

A similar study was performed by Piserchia et al (1998), in which they modeled T-phase conversion from an explosive source in the ocean, observed on the islands of Mururoa and Fangataufa in the South Pacific Ocean. They used ray tracing instead of a modal solution, and calculated Green's functions along a vertical boundary in order to propagate the source onto the islands. They found that the T-phase on land consisted of two P waves followed by two Rayleigh waves, where the multiple arrivals are identified as coming from different conversion points. The calculation was performed for a dominant frequency of 6 Hz, and the calculated P and Rayleigh waves were found to be comparable in size. Talandier and Okal (1998) studied conversion of T-phases on steep island slopes using data from the Polynesian Seismic Network and found from the observations and ray tracing arguments that the T-phase consisted primarily of P-waves at distances greater than 9 km from the conversion point. At closer distances, they found that the T-phase was more complex and composed primarily of S-waves and surface waves. They also suggested that only surface wave conversion would occur for slopes with angles of less than 16 degrees.

CONCLUSIONS AND RECOMMENDATIONS

We have used observations of T-phases underwater and on land to directly measure the transmission of energy from ocean to land, and have performed numerical simulations of T-phase propagation from ocean to land to obtain a better understanding of this process. The observations show that there is a significant decline in spectral amplitude with frequency on land compared to observations in the ocean. The observations also show that T-phases propagate primarily as P-waves once they are well inland. The numerical simulations provide considerable insight into the phenomena that occur when hydroacoustic waves propagate onto land. The calculations reproduce the spectral degradation observed in Coastal California stations. The calculations also suggest that strong surface waves may be present in T-phases observed near the coast while body waves may be the dominant phase farther inland.

ACKNOWLEDGEMENT

We thank Marcia McLaren of Pacific Gas and Electric for the use of her data and for pointing out to us the large T-phases from the Loihi events.

REFERENCES

- Cook, R. W. and J. L. Stevens (1998), "TP Phase Observations at the pIDC," Transactions of the American Geophysical Union, v. 79, P. F558, November.
- D'Spain, G. L., L. P. Berger, W. A. Kuperman, J. L. Stevens, and G. E. Baker (1999), "Normal mode composition of earthquake T-phases," submitted to Pure and Appl. Geophys.
- Mooney, W. D., G. Laske and T. Guy Masters (1998), "Crust 5.1: A global crustal model at 5°x5°," Journal of Geophysical Research, 103, 727-747.
- Piserchia, P. F., J. Virieux, D. Rodrigues, S. Gaffet and J. Talandier (1998), "Hybrid numerical modelling of T-wave propagation: application to the Midplate experiment," Geophys. J. Int., V. 133, pp 789-800.
- Stevens, Jeffrey L., G. Eli Baker, Ron W. Cook, Gerald D'Spain, Lewis P. Berger, and Steven M. Day (1999), "Empirical and Numerical Modeling of T-Phase Propagation from Ocean to Land", submitted to Pure and Applied Geophysics.
- Stevens, J. L. and K. L. McLaughlin (1997), "Improved Methods for Regionalized Surface Wave Analysis," Maxwell Technologies Final Report submitted to Phillips Laboratory, MFD-TR-97-15887, September.
- Talandier, J. and E. A. Okal (1998), "On the mechanism of conversion of seismic waves to and from T waves in the vicinity of island shores," Bull. Seism. Soc. Am., V.88, pp. 621-632.